2024 IEEE International Conference on Robotics and Automation (ICRA 2024)
May 13-17, 2024. Yokohama, Japan

Model-Free Control of a Class of High-Precision Scanning Motion Systems with Piezoceramic Actuators

Yazan M. Al-Rawashdeh[1] Mohammad Al Saaideh[1] Marcel F. Heertjes[2] Mohammad Al Janaideh[1,3]

***Abstract*— To enhance the precision of coarse long-stroke motion axes, complementary short-stroke fine positioning stages are usually introduced. Being mechanically attached, the motion of the combined positioning stages needs to be controlled and synchronized. Therefore, typically suitable model-based controllers of fine stages are designed according to the *sophisticated* models and identification techniques used. Due to their appealing features, Piezocermamic-based fine positioning stages were successfully utilized in many applications, which recently sparked their use in high-acceleration motion found in wafer scanners, for example, where high-precision motion is required despite the resulting high inertial forces involved. Unfortunately, hard nonlinear behavior is associated with piezoelectric actuators, which adds to the complexity of modeling, control, and synchronization processes. To overcome such a burden, in this study, the design procedure of a model-free control and synchronization technique of piezocermamic-based fine positioning stages is introduced and verified experimentally using a representative precision motion system comprising a planner stage and a uni-axial fine stage under step-and-scan trajectories commonly used in wafer scanners. Despite its *simplicity*, the herein proposed design procedure can be seamlessly extended to other robotics and automation applications.**

I. Introduction

When designing motion systems with nanometer precision accuracy, it is possible to combine coarse and fine positioning stages that complement each other precision and tracking capabilities. For example, in a dual-stage motion system, the coarse stage travels long distances in the meters range, and therefore, is known as the long-stroke (LS), while the fine stage travels shorter distances in the micro-meter range, and therefore, is known as the short-stroke (SS) [1]–[4]. From a robotics perspective, the resulting LS-SS motion system can be viewed as an open serial chain [5], and correspondingly, further analysis can be carried out if needed. Note that in a LS-SS configuration, the end-effector or payload is attached to the SS stage. Many applications have benefited from such a configuration, such as haptic feedback [6]- where the user establishes the LS motion and the piezo-actuated stage establishes the SS motion-, and chip industries [7]. For example, nanometric integrated circuits (ICs) are produced using wafer scanner machines, where replicas of ICs images are projected onto a silicon disk coated with a light-sensitive material [7], known as a *wafer*, with the ICs patterns located on a quartz plate *mask* [8]. In principle, step-and-scan motion trajectories are used to scan small rectangular areas of the wafer, known as *dies* during the scanning process. Next dies are reached through stepping, i.e. stepping process, [9]. While the stepping phase can be done as fast as possible under high acceleration motion profiles, scanning is done with a predetermined constant velocity. To make up for the precision loss at high acceleration rates, additional stages might be needed or used. The involvement of more stages means more weight to add, and therefore, in next-generation wafer scanners, for example, the integration of lightweight stages actuated in a fast and accurate manner is being sought. Recently, the use of piezoceramic actuators (piezo actuator) to actuate flexure-guided piezo stages as SS is becoming more popular [3], [10].

Due to its lightweight construction, a piezo actuator can move with subnanometer resolution very fast [11]. From a control perspective, a piezo actuator is controlled using mixed compliance compensation [3], and inversion-based [11] feedforward controller [12], just to name a few. Despite its associated advantages, a piezo actuator suffers from creep, vibration, and hysteresis effects that need to be compensated for [3], [11]. Model-based control techniques adopt suitable models that capture the nonlinear behaviours of the nanopositioning actuators such as Rate-dependent Prandtl-Ishlinskii (RDPI) hysteresis model [13], [14], and Dahl model-based hysteresis compensation [15] with a system structure described by the Hammerstein-Wiener system. The Hammerstein-Wiener system structure comprises a linear dynamics subsystem sandwiched by input and output (hard) nonlinearities [16]. Consequently, the involved model parameters are identified [16]; however, their values are hard to identify accurately [17]. This will hinder the synchronization of the LS and SS motions, in which the LS tracking error is usually fed- as is- to the SS controller [3].

II. Related Work and Main Contributions

In this study, we *utilize* the activator-inhibitor trajectory generator developed in [18] as a *model-free input shaper* of the SS stage, realized using piezo actuators. Its synchronization with LS motion will also be discussed. Moreover, its performance will be compared to the model-based RDPI model studied in [19]. Detailed dynamical modeling of dual-stage systems can be found in the literature [3], [20].

Mainly, in this study we consider:

- the integration of the LS of an existing precision motion system with the SS stage to build a dual-stage position-

[1]Department of Mechanical and Mechatronics Engineering, Memorial University, St. John's, NL A1B 3X5, Canada. {yalrawashdeh, mialsaaideh,maljanaideh}@mun.ca

[2] Marcel Heertjes is with ASML and Department of Mechanical Engineering at Eindhoven University of Technology, 5612 AZ Eindhoven, Netherlands, marcel.heertjes@asml.com

[3]School of Engineering, University of Guelph, Guelph, ON N1G 2W1, Canada, and with the Department of Mathematics, Czech Technical University, 166 36 Prague 6, Czechia (email: maljanai@uoguelph.ca)

ing system that can provide enhanced sub-nanometer accuracy,
- proposing a model-free active-inhibit trajectory generator that modifies the desired trajectories such that the tracking performance of the piezo-actuated SS is enhanced, and
- enhancing the scanning performance of the dual-stage system under a particular step-and-scan trajectory used mainly in wafer scanners.

III. Problem Formulation

A. Short-stroke system description

Consider the Hammerstein-Wiener system (Σ_1) depicted in Fig. 1, where the *unknown* dynamics is given as a cascade connection of an input nonlinearity $\mathcal{M}$, a linear dynamical part G_p, and an output nonlinearity $\mathcal{N}$. Interestingly, Σ_1 can be used to model the dynamics of motion systems exhibiting non-smooth nonlinearity such as hysteresis, dead-zone, saturation, and backlash that usually limit the system performance [16]. The system Σ_1 is controlled using a feedforward controller (FF), and is subjected to an external *unknown* disturbance $d(t)$. Other controllers can be used, including feedback-based controllers [21]. In general, it is intended to minimize the tracking error $(e(t) = p_d(t) - p_a(t))$ between the desired position $p_d(t)$ and the actual system response $p_a(t)$. The FF controller can be as simple as a static gain, or a more sophisticated internal model controller that inverts the Hammerstein-Wiener system under the desired command input, $p_d(t)$ such as done using RDPI hysteresis model [13], [14], and Dahl model-based hysteresis compensation [15]. Clearly, when $d(t) \neq 0$, the performance under only the FF controller will deteriorate, and as a remedy closed-loop controllers can be used instead such as retrospective cost adaptive control (RCAC) [21] especially when $d(t)$ is unknown. In that case, model-based control techniques that depend on estimates of Σ_1 dynamics might be limited, especially under open-loop control configurations. Therefore, a model-free control technique is investigated in this study. Note that $p_d(t)$ along with any needed i^{th} time derivative $(p_d^{(i)})$ are externally supplied, $u(t)$ is designed, $v(t), w(t)$ are inaccessible, i.e., unknown intermediate signals [16], [22], $d(t)$ is unknown, and $p_a(t)$ is assumed to be observable along with any needed i^{th} time derivative $(p_a^{(i)})$ being readily available for measurements or can be estimated using model-free observers such as high-gain observers [23], [24].

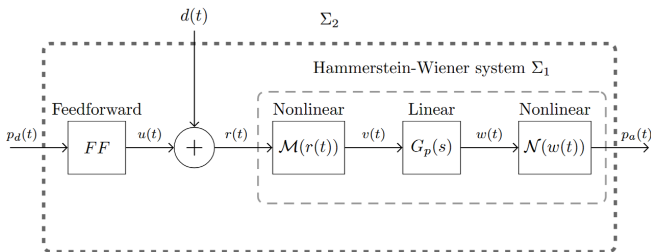

Fig. 1: Hammerstein-Wiener system Σ_1 with unknown input and output nonlinearities, subjected to external disturbance $d(t)$, and controlled using a feedforward controller FF.

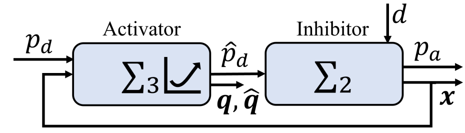

Fig. 2: Block diagram representations of the *controlled* Hammerstein system under $\Sigma_3 \leftrightarrow \Sigma_2$ head-to-tail interaction.

B. Model-free trajectory generation system

Adopting input-output perspective from $p_d(t)$ to $p_a(t)$ yields the system Σ_2 depicted in Fig. 1. According to the herein proposed approach, instead of adjusting $u(t)$ directly, a modified version of $p_d(t)$, i.e., $(\hat{p}_d(t))$, obtained by the *trajectory generator system* (Σ_3) is utilized, which results in minimizing the tracking error $e(t) = p_d(t) - p_a(t)$ as will be demonstrated here. Consequently, maintaining or enhancing the performance of Σ_2 under FF- or other used control techniques-when $d(t) \neq 0$ and/or Σ_1 dynamics are unknown is made possible. This means that any existing control loops are kept intact as long as Σ_2 is *input-to-state stable* [25], [26]. The head-to-tail interaction between Σ_2 and Σ_3 systems is depicted in Fig. 2.

Remark 1: Interestingly, the herein proposed approach can be applied to the LS as well. However, this will be investigated in future work.

1) Error estimates: Let $p_d^{(i)} = q_{i+1}$, and $p_a^{(i)} = x_{i+1}$ with $i = 0, 1, \cdots, n$ with $n \geq 1$. To make Σ_3 aware of Σ_2 tracking error $e = q_1 - x_1$, let the dynamics of the tracking error *estimates* $(\hat{e}_i)$ be given according to the following state estimator (observer) [18]

$$\begin{aligned} \dot{\hat{e}}_i &= \hat{e}_{i+1} + \beta_i \ (x_1 - q_1), \ i = 1, 2, \cdots, n-1 \\ \dot{\hat{e}}_n &= \hat{\sigma} + \beta_n \ (x_1 - q_1) + \beta_0 \ (x_{n+1} - q_{n+1}) \\ \dot{\hat{\sigma}} &= \beta_{n+1} \ (x_1 - q_1) \end{aligned} \tag{1}$$

with constants $\beta_i > 0 \in \mathbb{R}, i = 0, 1, \cdots, n+1$ are chosen such that (1) is stable, where β_0 is chosen to reflect the dependency on the available measurements (or estimates) of Σ_1. For example, when acceleration measurements are available, $1 \leq n \leq 2$ can be used in (1) under which Σ_3 will *activate* Σ_2 using the *modified* desired input $(\hat{p}_d)$, and Σ_2 will *inhibit* Σ_3 using $\hat{e}_1$ in a head-to-tail activator-inhibitor interaction. Ultimately, it is desired to reduce the tracking error $e_1 = p_d - x_1$ by re-adjusting p_d such that $x = [x_1, x_2, \cdots, x_{n+1}]^{\mathrm{T}}$ meets any imposed motion requirements. Let $q = [q_1, q_2, \cdots, q_{n+1}]^{\mathrm{T}}$, and $\hat{q} = [\hat{q}_1, \hat{q}_2, \cdots, \hat{q}_{n+1}]^{\mathrm{T}}$ with $\hat{q}_1$ be given as [18]

$$\hat{p}_d(t) \equiv \hat{q}_1 = q_1(t) - \hat{e}_1(t) \tag{2}$$

and other *modified* kinematical quantities given as [18]

$$\hat{q}_i = q_i(t) - \hat{e}_i(t), \ i = 2, \cdots, n+1 \tag{3}$$

Therefore, in the frequency domain and using the Laplace operator (s) with zero initial conditions, (1) is given as [18]

$$\hat{e}_1 = \frac{(\beta_0\, s^{n+1} + \beta_1\, s^n + \beta_2\, s^{n-1} + \cdots + \beta_{n+1})\,(x_1 - \hat{q}_1)}{(1+\beta_0)\, s^{n+1} + \beta_1\, s^n + \beta_2\, s^{n-1} + \cdots + \beta_{n+1}} \\ = G_e(s)\,(x_1 - \hat{q}_1) \tag{4}$$

Using (2) in (4), yields [18]

$$x_1 = q_1 + \left\{ \frac{1 - G_e(s)}{G_e(s)} \right\} \hat{e}_1 \tag{5}$$

Consequently, the constants $\beta_i \in \mathbb{R}$ should be chosen such that (1) is globally uniformly asymptotically stable, and $||G_e(j\,\omega)||_\infty$ is *ideally* close to unity $\forall\omega$ in the frequency domain of interest in which $|G_e(s)| = 0\,\mathrm{dB}$ and $\angle G_e(s) = 0$. Doing so results in $x_1 = q_1$ as required. Moreover, $\beta_i \in \mathbb{R}$ must yield a dynamically friendly $\hat{q}_i, i = 1, \cdots, n+1$ given in (3) such that any imposed kinematical constraints on Σ_1 are met. Interestingly, (1) seems to be linked to RCAC [21], with the exception that the former can be *easily* designed off-line especially when the operating frequency range of the desired position signal $p_d(t)$ is predictable as can be found in repetitive motion profiles found in wafer scanners [4], for example. Comparing both techniques is beyond the scope of this investigation.

2) Stability of the activator-inhibitor system: According to lemma 4.7 in [27] and assuming Σ_2 to be input-to-state stable under the used control technique, and the origin of Σ_3, i.e., (1), is globally uniformly asymptotically stable, then the origin of the cascaded system Σ_2 and Σ_3 is globally uniformly asymptotically stable.

C. Long-stroke desired signal

Consider the generalized fillet motion profile [28] depicted in Fig. 3, which can be used to design the desired signal (p) as the step-and-scan trajectory meant for wafer scanners, i.e. step along x-axis, and scan along the y-axis. Using third-order polynomials with *switched* coefficients, p can be given as [19]

$$p(t) := \begin{cases} x_d\,(t_x) = \alpha_0^k + \alpha_1^k\, t_x + \alpha_2^k\, t_x^2 + \alpha_3^k\, t_x^3 \\ y_d\,(t_y) = \beta_0^q + \beta_1^q\, t_y + \beta_2^q\, t_y^2 + \beta_3^q\, t_y^3, \end{cases} \tag{6}$$

with $t_{\{x,y\}} = \left(t - t_{0_{\{x,y\}}}\right)$, $t_{0_{\{x,y\}}}$ denotes the trajectory time shift in the x, y motion, and the *switched* coefficients α_l^k, β_l^q with $l = 0, 1, 2, 3$ in the k, q intervals are symbolically given in [28]. These switched coefficients are functions of the *maximum acceleration value* ($a^{max}_{\{step,scan\}}$) given in $\mathrm{m/s^2}$, the time interval of acceleration and deceleration (T_1), the interval of constant acceleration (T_2), the constant speed intervals ($D, d \equiv T_w$) all given in s, and the scaling factors ($s_{\{step,scan\}} > 0$) that are taken here as 1 and thus absent in the current formulation.

The step-and-scan trajectory can be characterized by several key features- as discussed in [28], [29]- among which the *scanning phase pitch size* (P_{scan}), and the constant *scanning speed* (V_{scan}) given as [28]

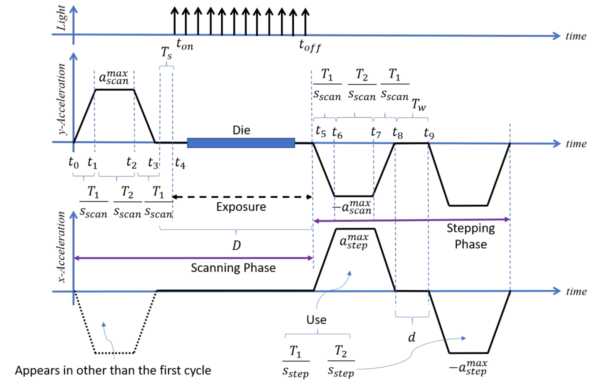

Fig. 3: Fillet acceleration trajectories along with the light source activation timing, resulting in a step-and-scan motion of one die [28].

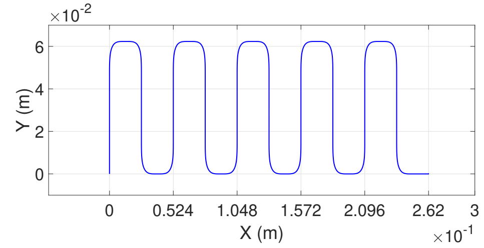

Fig. 4: A Step-and-scan motion profile of 10 dies [19].

$$P_{scan} = V_{scan}\,(2\,T_1 + T_2 + D) \\ V_{scan} = a^{max}_{scan}\,(T_1 + T_2), \tag{7}$$

also the *stepping phase pitch size* (P_{step}) given as [28]

$$P_{step} = a^{max}_{step}\,(T_1 + T_2)\,(2\,T_1 + T_2 + d) \tag{8}$$

Consider the step-and-scan motion of 10 dies as shown in Fig. 4, where $P_{scan} = 0.0623125\,\mathrm{m}$, $P_{step} = 0.026\,\mathrm{m}$, $T_1 = 0.04285\,\mathrm{s}$, $T_2 = 0.040476\,\mathrm{s}$, $D = 0.123059\,\mathrm{s}$, $d \equiv T_w = 0.020\,\mathrm{s}$, $a^{max}_{step} = 2.14285\,\mathrm{m/s^2}$, and $a^{max}_{scan} = 3\,\mathrm{m/s^2}$. Using these values, the tracking error of the LS stage (e_{LS}) under the realized fillet profile can be obtained. Its frequency contents will be instrumental when (4) is designed, as will be discussed shortly.

D. Problem Statement

As in [19], and given the previous information, introduce a piezo-actuated SS stage along with its controller to the existing LS stage such that the positioning error of the resulting dual-stage system is minimized during the step-and-scan motion, at least along the scanning direction.

IV. Dual-stage Motion System

A. Long-Stroke and Short-Stroke Stages

The LS stage used in this study is A-322 PIglide HS XY Planar Scanner with a resolution of $1\,\mathrm{nm}$, A-824 ACS Motion Controller, three ironless zero-cogging brushless 3-phase linear motors in an H-configuration [20], and air bearing levitation system, all arranged in a gantry configuration

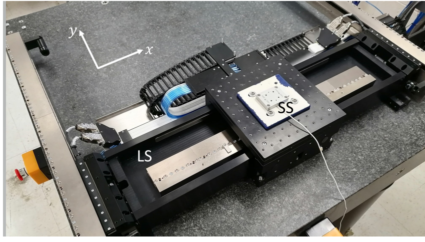

Fig. 5: The used long-stroke LS, and the short-stroke SS aligned in the x-direction.

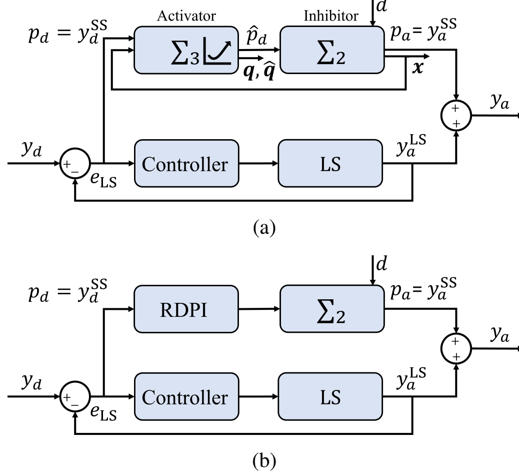

Fig. 6: The block diagram of the LS-SS integration under (a) $\Sigma_3 \leftrightarrow \Sigma_2$ interaction, and (b) RDPI model [19], in the y-direction, where Σ_2 denotes the SS piezo-actuated stage.

supported by a passive anti-vibration system. The available feedback signals are the position, velocity, acceleration, and tracking error in x and y directions.

The SS stage used in this study- due to availability- is a Nano-OP30 uni-axial nanopositioning stage driven by a piezo actuator with a motion range of 30 μm; the stage has an internal position sensor with a resolution of $0.06\,\text{nm}$. When the step-and-scan profile is involved, the SS stage is aligned with the LS y-axis, i.e., the scanning direction. Note that the effect of the LS motion on the SS motion was thoroughly studied in [19]. The LS-SS stages used in this study are shown in Fig. 5. Despite being applicable to SS stages in the z-direction, only motion along the x and y directions will be studied separately due to available hardware components.

B. Synchronous operation (short-stroke desired signal)

Let y_d, y_a denote the desired and actual positions of the dual-stage system, $\{y_d^{\text{SS}}, y_a^{\text{SS}}\}$ the desired and actual positions of the SS, and y_a^{LS} the actual position of the LS all in the y-direction. Setting $y_d^{\text{SS}} = e_{\text{LS}_y}$, the LS error e_{LS}, the SS error (e_{SS}), and the total tracking error (e_{f_y}) are related by [19]

$$\begin{aligned} e_{\text{LS}_y}(t) &= y_d(t) - y_a^{\text{LS}}(t) \\ e_{\text{SS}_y}(t) &= e_{\text{LS}_y}(t) - y_a^{\text{SS}}(t) \\ y_a(t) &= y_a^{\text{LS}}(t) + y_a^{\text{SS}}(t) \\ e_{f_y}(t) &= y_d(t) - y_a(t) \equiv e_{\text{SS}_y}(t). \end{aligned} \tag{9}$$

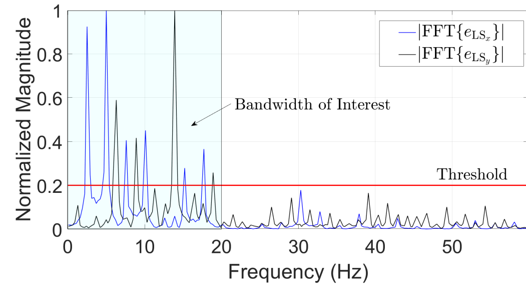

Fig. 7: Single-sided amplitude spectrum of e_{LS_x} and e_{LS_y} of the 10 dies scanning profile depicted in Fig. 4.

where similar relations can be derived for the motion along the x-direction. Therefore, the SS errors e_{SS_x} and e_{SS_y} can be used to assess the performance of the dual-stage system under the herein-proposed approach compared to the RDPI model [19].

C. Performance assessment

The low-frequency components of e_{SS_y}- for example- can be captured using the error moving average (MA_y) [8]. This metric reflects the wafer scanner ability to expose two images on top of each other, i.e., overlay error. At high frequencies, the moving standard deviation (MSD_y) is used instead mainly to assess the image contrast during exposure [8]. In actual wafer scanners, typical values of a 38-nm half-pitch lithography would be $\text{MA} \leq 1$ nm, and the MSD ≤ 7 nm [8] during the constant speed scanning motion.

Similarly, in this study, both MA_y and MSD_y are used to assess e_{SS_y} during scanning motion in the y-direction, and they are given as [30]

$$\begin{aligned} \text{MA}_y(t) &= \frac{1}{T}\int_{-\frac{T}{2}}^{\frac{T}{2}} e_{\text{SS}_y}(t)\,dt \\ \text{MSD}_y(t) &= \sqrt{\frac{1}{T}\int_{-\frac{T}{2}}^{\frac{T}{2}} \left(e_{\text{SS}_y}(t) - \text{MA}_y\right)^2 dt} \end{aligned} \tag{10}$$

where T denotes the time interval of interest, which is usually taken as the constant speed scanning motion [8], i.e., D shown in Fig. 3. Similarly, MA_x and MSD_x can be used to assess e_{SS_x} during stepping motion in the x-direction.

V. Experimental Results

The SS dynamics were modeled in [19], and since the stage has only a position sensor with a resolution of $0.06\,\text{nm}$ that provides clean measurements of $p_a(t)$, any needed $p_a^{(i)}$ is obtained using numerical differentiation. The same applies to $p_d(t)$. Also, the FF controller used in Σ_2 is a static gain, i.e., $1/1.5045\,(\text{V}/\mu\text{m})$, based on [19].

Starting with the desired position signals $y_d(t)$ and $x_d(t)$ depicted in Fig. 4 and given by (6), the associated frequency contents can be determined using fast Fourier transform (FFT), and consequently the bandwidth of interest can be determined as pictured in Fig. 7. Accordingly, $G_e(s)$ in (4) can be designed, and its bandwidth ($\text{BW}\{G_e(s)\}$) can be assigned. For example, as depicted in Fig. 4, the frequency

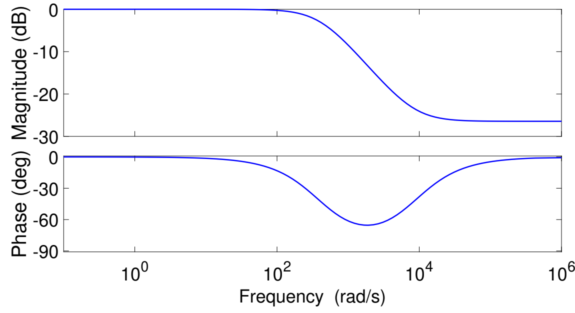

Fig. 8: The Bode plot of G_e utilizing the velocity estimates.

contents of both e_{LS_x} and e_{LS_y} have a significant contribution below $20\,\mathrm{Hz}$. According to Fig. 1, both e_{LS_x} and e_{LS_y} can serve as the input to Σ_2 once the *available* SS stage is aligned in their designated directions, i.e., $p_d(t) \equiv e_{\mathrm{LS}_x}(t)$ or $p_d(t) \equiv e_{\mathrm{LS}_y}(t)$, based on the LS-SS configuration depicted in Fig. 6(a).

Using the velocity estimates with $n = 1$ in (4) yields

$$G_e(s) = \frac{0.05\,s^2 + 425\,s + 100}{1.05\,s^2 + 425\,s + 100} \tag{11}$$

and its Bode plot is depicted in Fig. 8. The same $G_e(s)$ given in (11) will be used to handle e_{LS_x} and e_{LS_y}.

Recalling Fig. 6, and by utilizing the block diagrams of the LS-SS integration under $\Sigma_3 \leftrightarrow \Sigma_2$ interaction, and RDPI model [19], the tracking errors associated with the fillet profile shown in Fig. 4 are depicted in Fig. 11. According to Fig. 9(a), when no disturbance is active, i.e., $d = 0$, both the model-free $\Sigma_3 \leftrightarrow \Sigma_2$ interaction and the model-based RDPI model resulted in almost a similar tracking error considering the motion along the x-direction. However, when $d \neq 0$, the model-free $\Sigma_3 \leftrightarrow \Sigma_2$ interaction outperforms the model-based RDPI model due to the former's awareness of the actual SS response through the available feedback measurements. Similar results can be deduced about the tracking error along the y-direction as can be seen from Fig. 9(b). The disturbance d is *imitated* using a pulse of amplitude $0.3\,\mathrm{V}, \forall t \in [4, 5]$ s, where the piezo amplifier internally provides a gain of 10 to this applied disturbance. The effects on the desired signal in the x-direction can be seen from Fig. 10, where interestingly the control signal $r(t)$ is not affected by $d(t)$. Recalling Fig. 1, Σ_3 changes the desired signal $q_1 \equiv p_d$ such that the resulting control signal $r(t) = u(t) + d(t)$ is not affected by $d(t)$. Note that this will not be the case when the disturbance appears at the output side, i.e., p_a. This case will be examined in a separate study.

Using (10) with T covering the whole range of motion, i.e., about $4\,\mathrm{s}$, the performance of the dual-stage system under $\Sigma_3 \leftrightarrow \Sigma_2$ interaction compared to the RDPI model [19] is assessed when $d(t) = 0$. As shown in Fig. 11, $\Sigma_3 \leftrightarrow \Sigma_2$ interaction outperforms the RDPI model at low frequencies as captured by the MA metric, while both almost do nothing to $e_{mathrmLS_x}$ and $e_{mathrmLS_y}$ at higher frequencies as captured by the MSD metric. Only a sampling rate of $1\,\mathrm{ms}$ was used in this study. The effect of using a higher sampling rate, and higher value of n in (4) on specifically the MSD performance metric will be investigated in a future work.

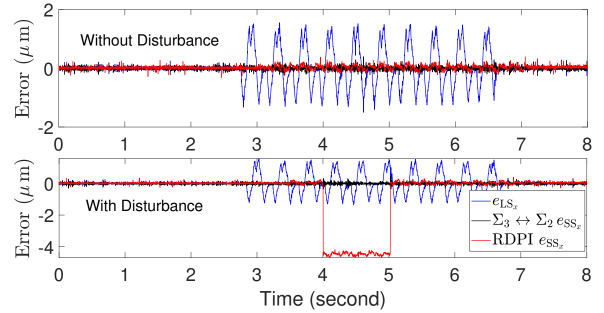

(a)

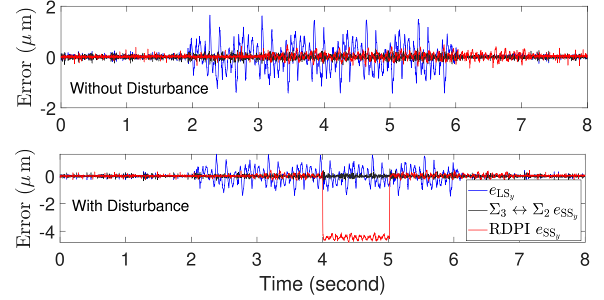

(b)

Fig. 9: The tracking errors of the LS-SS system along (a) x, and (b) y directions, with and without disturbance d.

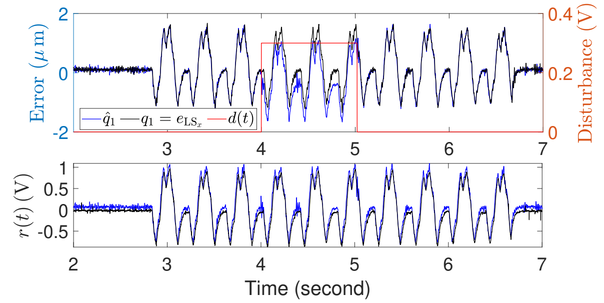

Fig. 10: The (top) SS modified tracking error $\hat{q}_1$ (blue) in the x-direction when $d \neq 0$, and (bottom) the corresponding control input $r(t) = u(t) + d(t)$ both compared to the case when $d = 0$ (black).

VI. Conclusion

A model-free input shaper of a uni-axial fine positioning stage was introduced. The integration of the fine stage with an existing long-stroke stage resulted in a dual-stage positioning system whose tracking performance was enhanced under the proposed technique. Simply, the proposed technique shapes the desired input signal, i.e., the tracking error of the long-stroke stage, to meet the dynamical requirements of the driven fine stage even when disturbance is present. A comparison with the Prandtl–Ishlinskii inverse model revealed the advantages of the proposed model-free input shaper whose performance was relatively better than the used model-based method especially at low frequencies of the command signal as revealed by the moving average performance metric. A design procedure for the proposed

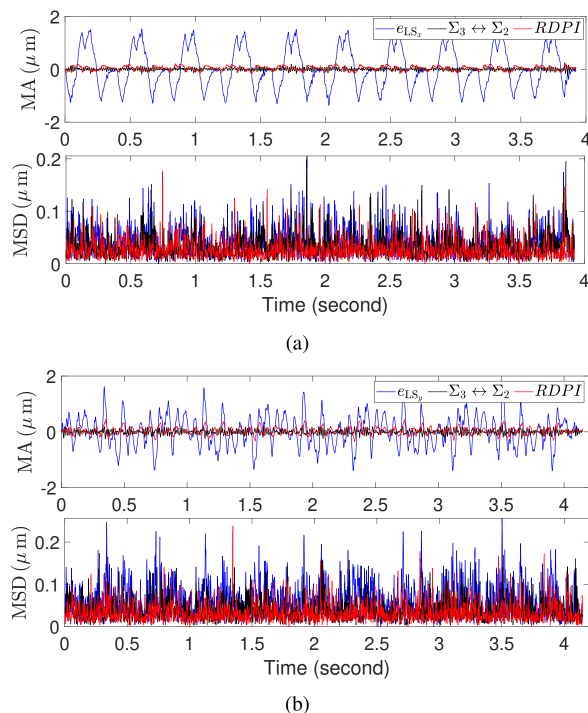

Fig. 11: The MA and MSD tracking error performance metrics of the LS-SS system along (a) x, and (b) y directions, without disturbance, i.e., $d = 0$.

method was also provided. Future work will be directed towards improving the proposed input shaper performance at higher frequencies of the command signal based on the moving standard deviation performance metric.

References

[1] A. Mitrovic, W. Nagel, K. Leang, and G. Clayton, "Closed-loop range-based control of dual-stage nanopositioning systems," *IEEE/ASME Transactions on Mechatronics*, vol. 26, pp. 1412–1421, 2020.

[2] D. Guo, W. Nagel, G. Clayton, and K. Leang, "Spatial-temporal trajectory redesign for dual-stage nanopositioning systems with application in AFM," *IEEE/ASME Transactions on Mechatronics*, vol. 25, pp. 558–569, 2020.

[3] C. Barros, H. Butler, J. van de Wijdeven, and R. Tóth, "On feedforward control of piezoelectric dual-stage actuator systems," *in 60th IEEE Conference on Decision and Control (CDC)*, pp. 5588–5594, 2021.

[4] Y. Al-Rawashdeh, M. Al Janaideh, and M. Heertjes, "Kinodynamic generation of wafer scanners trajectories used in semiconductor manufacturing," *IEEE Transactions on Automation Science and Engineering*, vol. 20, pp. 718–732, 2022.

[5] A. Jain, "Multibody graph transformations and analysis: part i: tree topology systems," *Nonlinear dynamics*, vol. 67, pp. 2779–2797, 2012.

[6] P. Zhang, M. Kamezaki, Y. Hattori, and S. Sugano, "A wearable fingertip cutaneous haptic device with continuous omnidirectional motion feedback," in *2022 International Conference on Robotics and Automation (ICRA)*. IEEE, 2022, pp. 8869–8875.

[7] M. Heertjes, B. Van der Velden, and T. Oomen, "Constrained iterative feedback tuning for robust control of a wafer stage system," *IEEE Transactions on Control Systems Technology*, vol. 24, no. 1, pp. 56–66, 2016.

[8] H. Butler, "Position control in lithographic equipment," *IEEE Control Systems Magazine*, vol. 31, no. 5, pp. 28–47, 2011.

[9] C. Mack, *Fundamental principles of optical lithography: The science of microfabrication*. Hoboken, NJ, USA: John Wiley & Sons, 2008.

[10] Z. Chen, J. Shi, S. Zhu, X. Zhong, and X. Zhang, "Design and testing of a damped piezo-driven decoupled xyz stage," in *2021 IEEE International Conference on Robotics and Automation (ICRA)*. IEEE, 2021, pp. 6986–6991.

[11] K. Leang, Q. Zou, and S. Devasia, "Feedforward control of piezoactuators in atomic force microscope systems," *IEEE Control Systems Magazine*, vol. 29, pp. 70–82, 2009.

[12] A. Singh, T. Libby, and S. B. Fuller, "Rapid inertial reorientation of an aerial insect-sized robot using a piezo-actuated tail," in *2019 International Conference on Robotics and Automation (ICRA)*. IEEE, 2019, pp. 4154–4160.

[13] M. Al Janaideh and P. Krejčí, "Inverse rate-dependent prandtl–ishlinskii model for feedforward compensation of hysteresis in a piezomicropositioning actuator," *IEEE/ASME Transactions on mechatronics*, vol. 18, no. 5, pp. 1498–1507, 2012.

[14] M. Al Janaideh and O. Aljanaideh, "Further results on open-loop compensation of rate-dependent hysteresis in a magnetostrictive actuator with the prandtl-ishlinskii model," *Mechanical Systems and Signal Processing*, vol. 104, pp. 835–850, 2018.

[15] Q. Xu and Y. Li, "Dahl model-based hysteresis compensation and precise positioning control of an xy parallel micromanipulator with piezoelectric actuation," 2010.

[16] Z. Zhang, D. Zhang, H. Zheng, T. Huang, and Y. Xie, "Identification of a precision motion stage based on the hammerstein-wiener model," in *2019 Chinese Control Conference (CCC)*. IEEE, 2019, pp. 1637–1642.

[17] J. Wang and Q. Xu, "Precision tracking control of piezoelectric-driven motion system based on enhanced adrc," in *2020 39th Chinese Control Conference (CCC)*. IEEE, 2020, pp. 2626–2630.

[18] Y. M. Al-Rawashdeh, M. A. Saaideh, A. M. Boker, H. Eldardiry, M. F. Heertjes, and M. A. Janaideh, "Trajectory generation using activator-inhibitor systems," in *IEEE Conference on Decision and Control (CDC)*. IEEE, 2023.

[19] Y. M. Al-Rawashdeh, M. A. Saaideh, and M. A. Janaideh, "Using piezoceramic-actuated stages in precision long-stroke motion systems: A design procedure," in *IEEE/RSJ International Conference on Intelligent Robots and Systems (IROS)*. IEEE, 2023.

[20] Y. Al-Rawashdeh, M. Al Janaideh, and M. Heertjes, "On characterization of a generic lithography machine in a multi-directional space," *Mechanism and Machine Theory*, vol. 170, pp. 1–23, 2022.

[21] M. Al Janaideh and D. S. Bernstein, "Adaptive control of uncertain hammerstein systems with hysteretic nonlinearities," in *53rd IEEE Conference on Decision and Control*. IEEE, 2014, pp. 545–550.

[22] K. F. Aljanaideh, M. Al Janaideh, M. Rakotondrabe, M. Al Saaideh, A. M. Almomani, M. A. Bani Hani, and D. Kundur, "Identification of a class of precision motion systems with uncertain hysteretic nonlinearities," *International Journal of Control*, vol. 96, no. 8, pp. 1971–1988, 2023.

[23] D. Chowdhury, Y. K. Al-Nadawi, and X. Tan, "Hysteresis compensation using extended high-gain observer and dynamic inversion," in *Dynamic Systems and Control Conference*, vol. 51906. American Society of Mechanical Engineers, 2018, p. V002T24A005.

[24] H. K. Khalil, "High-gain observers in nonlinear feedback control," in *2008 International Conference on Control, Automation and Systems*, 2008, pp. xlvii–lvii.

[25] C. Jan and C.-L. Hwang, "Robust control design for a piezoelectric actuator system with dominant hysteresis," in *2000 26th Annual Conference of the IEEE Industrial Electronics Society. IECON 2000. 2000 IEEE International Conference on Industrial Electronics, Control and Instrumentation. 21st Century Technologies*, vol. 3. IEEE, 2000, pp. 1515–1520.

[26] S. Ibrir and C.-Y. Su, "Adaptive stabilization of a class of feedforward nonlinear systems subject to unknown backlash-hysteresis inputs," *IEEE Transactions on Control Systems Technology*, vol. 25, no. 4, pp. 1180–1192, 2016.

[27] H. K. Khalil, "Nonlinear systems third edition," *Patience Hall*, vol. 115, 2002.

[28] Y. Al-Rawashdeh, M. Al Janaideh, and M. Heertjes, "On step-and-scan trajectories used in wafer scanners in semiconductor manufacturing," *in 2021 IEEE/RSJ International Conference on Intelligent Robots and Systems (IROS)*, pp. 7580–7586, 2021.

[29] ——, "Kinodynamic generation of wafer scanners trajectories used in semiconductor manufacturing," *IEEE Transactions on Automation Science and Engineering*, vol. 20, pp. 718–732, 2023.

[30] M. Heertjes, "Data-based motion control of wafer scanners," *IFAC-PapersOnLine*, vol. 49, pp. 1–12, 2016.